Superconductor Science and Technology

Magnetization collapse in polycrystalline YBCO under transport current cycles

To cite this article: J L Giordano *et al* 2006 *Supercond. Sci. Technol.* **19** 385

View the article online for updates and enhancements.

Related content

- Smooth double critical state theory for type-II superconductors
H S Ruiz and A Badía-Majós
- Magnetic relaxation induced by transverse flux shaking inMgB_2 superconductors
J Luzuriaga, A Badía-Majós, G Nieva et al.
- Electromagnetics close beyond the critical state: thermodynamic prospect
A Badía-Majós and C López

Recent citations

- Magnetization Profiles of AC Type-II Superconducting Wires Exposed to DC Magnetic Fields
Bright Chimezie Robert and Harold Steven Ruiz
- Magnetic characteristics and AC losses of DC type-II superconductors under oscillating magnetic fields
B C Robert and H S Ruiz
- Computation of Losses in HTS Under the Action of Varying Magnetic Fields and Currents
Francesco Grilli *et al*

IOP ebooks™

Bringing together innovative digital publishing with leading authors from the global scientific community.

Start exploring the collection–download the first chapter of every title for free.

This content was downloaded from IP address 181.117.38.97 on 06/03/2021 at 16:36

INSTITUTE OF PHYSICS PUBLISHING SUPERCONDUCTOR SCIENCE AND TECHNOLOGY

Supercond. Sci. Technol. **19** (2006) 385–391 doi:10.1088/0953-2048/19/4/024

Magnetization collapse in polycrystalline YBCO under transport current cycles

J L Giordano[1], J Luzuriaga[2], A Badía-Majós[3], G Nieva[2] and I Ruíz-Tagle[4]

[1] Departamento de Ciencias de la Ingeniería, Universidad de Talca, Chile
[2] Centro Atómico Bariloche, CNEA, Instituto Balseiro, UNC, Argentina
[3] Departamento de Física de la Materia Condensada—ICMA, Universidad de Zaragoza, Spain
[4] Instituto de Química de Recursos Naturales, Universidad de Talca, Chile

E-mail: giordano@utalca.cl

Received 23 December 2005, in final form 3 January 2006
Published 7 March 2006
Online at stacks.iop.org/SUST/19/385

Abstract

We report measurements of the hysteretic magnetization of YBCO under superimposed transport current cycles, together with numerical simulations of magnetization and current density profiles in the corresponding parallel configuration. Field cooled (FC) and zero-field-cooled (ZFC) experiments were carried out on polycrystalline $YBa_2Cu_3O_{7-x}$ cylinders, with both the applied magnetic field and transport current in the axial direction, and the current cycled several times, around and above the dissipative threshold. As in previously reported multicomponent field configuration experiments, the magnetization is seen to collapse to a more stable state both in FC and ZFC, because of the interplay between the shielding and transport currents. The results of our numerical simulations are in good qualitative agreement with the measurements, and the competition between shielding and transport due to vortex-pinning interactions and equilibrium magnetization effects are shown to play an important role in the range of our experiments.

(Some figures in this article are in colour only in the electronic version)

1. Introduction

Vortex–matter interactions in pinned type-II superconductors are a complicated subject, due to the relevance of many physical phenomena. This is most noticeable in the case of high-T_c compounds due to the smallness of the superconducting coherence length. Interactions are highly sensitive to the material microstructure, thermal fluctuations, etc. Thus, when investigating the properties of the Schubnikov phase, even at a phenomenological level, one should start with the force between straight vortices and pinning sites [1], then consider crossing interactions between adjacent tilted vortices [2], and also include the equilibrium properties of the flux line lattice [3], thermal excitations [4], and possibly the influence of granularity in the case of high-T_c superconductors (HTSs) [5, 6].

However, depending on the experimental conditions, the theory may be highly simplified if one of the previous mechanisms prevails. For instance, the hysteretic properties for low temperatures $T/T_c \ll 1$ and moderate magnetic fields $H_{c1} \ll H \ll H_{c2}$ are nicely described by the simple and celebrated Bean's critical state model [1]. In this case, one basically assumes that vortex displacements away from equilibrium with pinning sites are highly dissipative. The critical state concept is still useful for situations in which vortices may be no longer simplified as straight lines and multicomponent fields within the superconductor are involved [7–10]. In fact, one can still invoke a *one-parameter* theory which successfully describes flux rotation and cutting interactions. A general critical state model, built on the restriction $J \leqslant J_c$ for the modulus of the current density, displays the properties of such experiments [11, 12]. However, some experimental observations may require a more complex theoretical scenario. For instance, the consideration of realistic situations important in many possible applications, involving applied field, transport current and temperatures not so far from T_c, requires further study.

In this paper, complementing previous work on HTSs [13, 14], we show results of magnetization measurements and

 © 2006 IOP Publishing Ltd Printed in the UK

simulations in a cylindrical geometry, with transport current applied parallel to the axis and also to the static magnetic field. We present and analyse new experimental data on $YBa_2Cu_3O_{7-x}$ cylinders, for $0.75 < T/T_c < 0.95$, when an externally controlled current is cycled, reaching the dissipative regime.

2. Sample and apparatus

Cylindrical samples of $T_c \approx 91$ K were prepared from YBCO powder, using standard prescriptions for HTSs. The specimens were isostatically pressed for 12 h, and sintered under O_2 atmosphere. The electric contacts were painted with Ag paste, and annealed for 10 h at 840 °C and 10 h at 450 °C.

As reported [13], a dedicated manual insertion utility probe and sample holder were designed for use in a commercial Quantum Design MPMS-5S (SQUID).

Simultaneous four-wire resistive (longitudinal transport) and inductive (axial magnetic moment) measurements can be performed without introducing distortions. Each sample was glued with varnish in the centre of a 112 mm sample holder, fabricated with four twisted copper AWG32 wires (0.203 diameter). The inductive quantity shown corresponds to the sample's magnetic moment per unit volume, the magnetization $\mu_0 M = (4\pi/10) \times (m_z/v)$ in millitesla (1 mT = 10 G), where m_z is the axial magnetic moment in erg/G ('emu') from the SQUID and v is the specimen volume in cubic centimetre. The applied magnetic strength H is expressed in terms of the magnetic induction $B = \mu_0 H$ in vacuum, in millitesla.

Field cooled (FC) and zero-field-cooled (ZFC) experiments were carried out using DC magnetic field in the range 0–150 mT, at $0.75 < T/T_c < 0.95$. Since the intragranular lower critical field is $B_{c1g} \sim 15$ mT [5, 6], this corresponds to the granular regime with $B_{max} \sim 10 B_{c1g}$.

In the experiments with transport cycles, the bias current was applied subsequent to setting up temperature and field. The current was cycled between −300 and +300 mA, in ±50 mA steps. The sample is 7.4 mm long, with a diameter of 1.22 mm, so the maximum global transport current density (calculated as if it was uniform) is about 25 A cm^{-2}.

3. Experimental results

Figure 1 combines the sample's diamagnetism together with transport losses in FC and ZFC experiments. In the lower part of the figure we show the power dissipation within the sample in a temperature sweep, with a fixed transport current of 100 mA and an applied magnetic field of 15 mT. Note that the onset of non-dissipative transport appears at lower temperature in the ZFC case, in which the shielding is higher. This property suggests a model in which transport and shielding current densities are not independently constrained.

In figure 2, the measured hysteresis loop at 80 K is shown. From the loop, at 15 mT, and using a uniform current Bean critical model, we obtain a critical current density around 1.25×10^3 A cm^{-2}. The equilibrium magnetization has been evaluated from the hysteresis loop ($(M_{up} + M_{down})/2$), and is shown in the lower part (solid line). The FC magnetization is also plotted in this graph, and was obtained independently, by

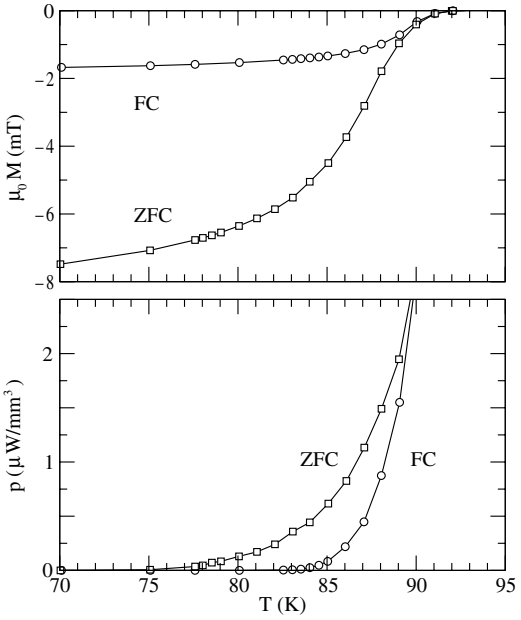

Figure 1. FC and ZFC comparison of magnetization (upper) and power dissipation per unit volume (lower) versus temperature for transport current $I = 100$ mA and applied magnetic field strength $\mu_0 H = 15$ mT.

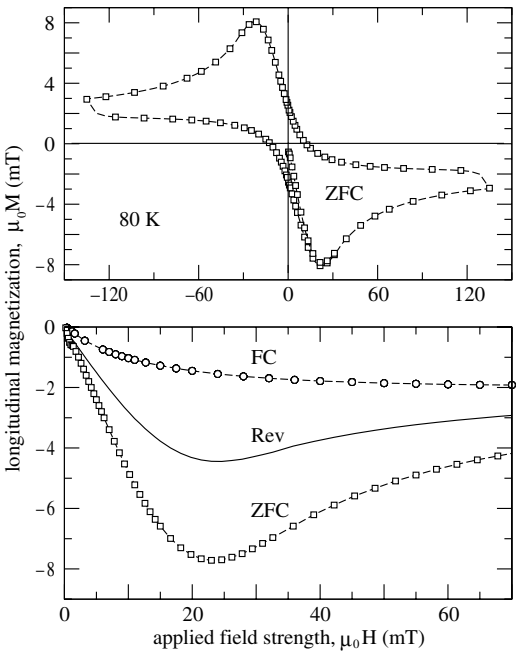

Figure 2. Upper: hysteresis loop of magnetization versus applied magnetic field at $T = 80$ K ($I = 0$ mA). Lower: FC, ZFC and reversible magnetization. Curves with symbols indicate direct experimental values, whereas the reversible curve (continuous line) was obtained from the hysteresis loop.

setting the field above T_c for each field value and then cooling the sample to 80 K, where the magnetization was measured.

Notice that the hysteresis loop is markedly *compressed* into quadrants II and IV, indicating the relevance of equilibrium magnetization effects. This is emphasized in the lower part of

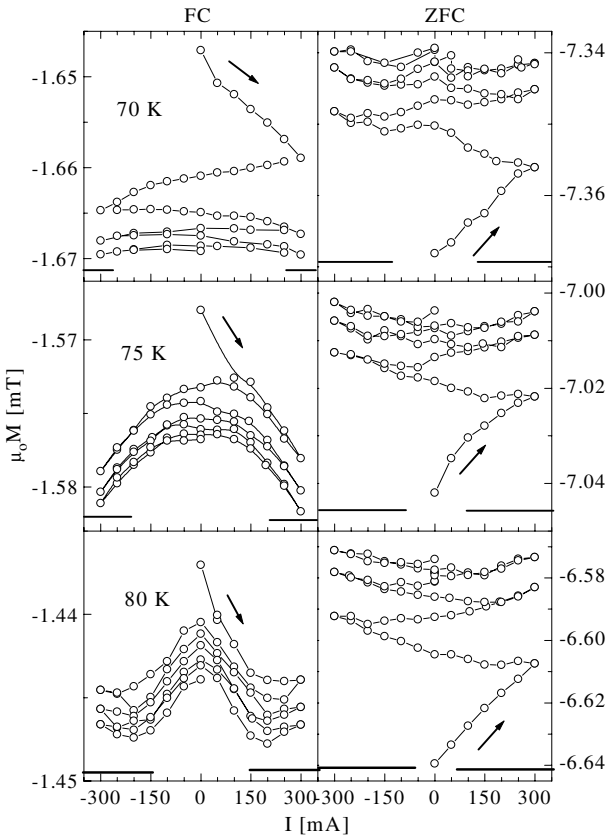

Figure 3. Summary of the magnetization versus current cycle behaviour in FC (left) and ZFC (right) experiments for $\mu_0 H = 15$ mT and different temperatures. The arrows indicate the direction of time evolution.

the figure, that shows the equilibrium and the two metastable states. In ZFC, the current induced by the sweeping field maintains a diamagnetic field profile, i.e. a Bean state, while in FC state some magnetic flux is trapped inside the sample, leading to reduced diamagnetism.

In figure 3, we show the effect of the transport current cycles on the magnetization, for three temperatures, with an applied field of 15 mT. In the graphs, the bars indicate the current range where the transport current is dissipative, that is, where we can detect a voltage across the electric contacts. It can be seen that the current reaches a dissipative regime along the cylinder axis, but there is still a magnetization component out of equilibrium, corresponding to a non dissipative Bean-like current.

The so-called *magnetization collapse* [12, 13] towards the thermodynamic equilibrium state is observed. The ZFC curves show an evolution from a more diamagnetic non-equilibrium state towards a less diamagnetic one, because the competition between transport and shielding currents affects the Bean profile, reducing the shielding capability. As a general trend, in the FC case, the evolution is again towards the equilibrium state. Nevertheless, here the magnetization becomes more diamagnetic, as the trapped flux is able to leave the sample as is shown by the simulations of the following section.

Although the number of physical phenomena is possibly higher from the microscopic point of view, the basic properties may be described at a phenomenological level based on an averaged critical state theory, modified by equilibrium magnetization effects in a simple form. Other aspects, such as the detailed description of granularity or time relaxation phenomena, may be regarded as second order corrections, and could be responsible for the qualitative differences observed in figure 3 for the different temperatures.

4. Theoretical framework

In this part, we describe the theoretical framework within which the experimental observations have been analysed. First, we develop a critical state formulation, built in terms of the variational statement posed in previous work [12]. This will account for hysteresis losses. In a second step, the theory will be upgraded in order to incorporate equilibrium magnetization effects, which are of importance within our experimental regime.

4.1. Critical state theory

The main complication of using a critical state formulation in multicomponent problems is that the direction of the current density vector $\vec{J}$ is unknown *a priori*. This difficulty may be dealt with in several forms. We have preferred a variational statement [12] in which both the direction and modulus of $\vec{J}$ as time goes by (field penetrates), are an output of the model. For the case under consideration, i.e. long cylinder with longitudinal field and transport current, the variational statement reads

$$\texttt{Minimize} \quad \frac{\mu_0}{2}\int_\Omega \|\vec{H}_{n+1} - \vec{H}_n\|^2 \,\mathrm{d}V, \qquad \vec{J}_{n+1} \in \Delta. \quad (1)$$

Here, $\vec{H}_n$ is the magnetic field at the time layer n and the restriction $\vec{J}_{n+1} \in \Delta$ applied to the volume of the superconductor. This is nothing but the *critical current* constraint, that will be used in the form $|\vec{J}| \leqslant J_c$ within this work. Ω is a cylinder with the same radius of the original one, and arbitrary length. For instance, one can consider unit length. On the other hand, the rotational and translational symmetry introduce the simplification

$$H_\rho = 0; \qquad J_\rho = 0$$

for the radial components of the fields within Ω.

Solving equation (1) for a given driving process requires us to define a finite element discretization suitable for representing the vector fields within Ω. Owing to the symmetry, the induced current density may be thought of as a set of co-axial cylindrical layers. Charges flow both along the Z-direction and in circular paths (see figure 4). Let us denote by the subscripts j and m two such layers. Let us also use the following notation for the cylindrical components of the current density within the jth layer:

$$\vec{J}_j \equiv (0, \phi_j, \zeta_j).$$

Then, by using Ampère's circuital law, one can show that equation (1) may be transformed (see the appendix) to a discretized minimization problem. Flux penetration in (or exit from) the sample is described by minimizing

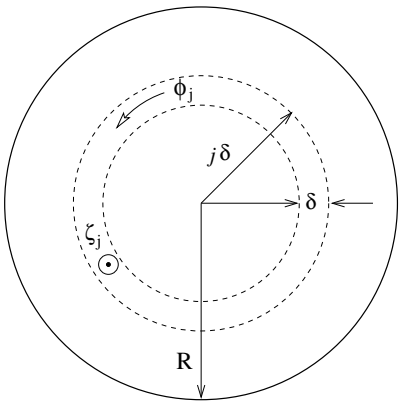

Figure 4. Sketch of the discretization scheme used in this work. The cross section of the cylinder is divided into N layers of width δ. Each of them carries a longitudinal current density ζ_j and an azimuthal component ϕ_j, as indicated in the picture.

$$\begin{aligned}\mathtt{F}(\{\phi_j\},\{\zeta_j\}) &= \tfrac{1}{2}\sum_{j,m}\left(\phi_j M^{\Phi}_{j,m}\phi_m + \zeta_j M^{\mathrm{Z}}_{j,m}\zeta_m\right)\\ &- \sum_{j,m}\left(\check{\phi}_j M^{\Phi}_{j,m}\phi_m + \check{\zeta}_j M^{\mathrm{Z}}_{j,m}\zeta_m\right)\\ &+ \sum_j\left(N^{\Phi}_j - \check{N}^{\Phi}_j\right)\phi_j. \end{aligned} \tag{2}$$

In order to simplify notation we have *superscripted* with '$\check{}$', the quantities referred to the previous time layer, and use plain style for their current values, in the iterative solution of the problem.

On the other hand, we have used the definitions

$$M^{\Phi}_{j,j} \equiv \tfrac{1}{2}j\left(j-\tfrac{1}{2}\right)$$

$$M^{\Phi}_{j,m} \equiv \tfrac{1}{2}\left[\mathtt{min}\{j,m\}\right]^2$$

$$N^{\Phi}_j \equiv \frac{H_0}{\delta}j^2$$

$$M^{\mathrm{Z}}_{j,j} \equiv \frac{j}{4} + j^2\sum_{k=j+1}^{N}\frac{1}{k}$$

$$M^{\mathrm{Z}}_{j,m} \equiv \frac{1}{2}\mathtt{min}\{j,m\} + jm\sum_{k=\mathtt{max}\{j,m\}+1}^{N}\frac{1}{k}.$$

H_0 denotes the magnetic field applied along the Z-axis.

We emphasize that for the case of interest, i.e. a constant bias field along the Z-axis, and cycles of transport current, the last term of equation (2) will become zero.

Finally, within the isotropic critical state model (the region Δ is a circle), minimization must be carried out under the restrictions

$$\begin{aligned}&\phi_j^2 + \zeta_j^2 \leqslant J_{\mathrm{c}}^2 \qquad \forall\ j\\ &\sum_j \zeta_j = I,\end{aligned} \tag{3}$$

related to the critical current threshold and to the bias transport current, respectively. As shown in previous work [11, 12], the solution of the variational statement for this kind of problem is always reached in the form $|\vec{J}| = J_{\mathrm{c}}$ (or 0).

We recall that the *isotropic restriction* for the current density has been already emphasized as a quite reasonable approximation for the flux dynamics of HTS ceramics [15].

4.2. Equilibrium magnetization effects

The simplest model for incorporating the equilibrium diamagnetic response consists of using surface discontinuity conditions for the magnetic flux density. Physically, this corresponds to neglecting the decay distance for London supercurrents, as compared to other relevant length scales, in particular, as compared to H/J_{c}. Thus, one associates a surface current density with the reversible response of the sample, and a volume *critical state* current density towards the centre. Then, within the volume of the sample we use the free space relationship $B = \mu_0 H$, and the critical state equations as displayed in the previous paragraphs.

Following reference [14] we assume a discontinuity for the magnetic field intensity

$$H(S^-) = H(S^+) - f H_{\mathrm{c1,g}} \tag{4}$$

with $S^{\pm}$ indicating a point close to the surface, either within the superconductor or outside, and f a phenomenological constant. On the other hand, the angle of the magnetic induction relative to the Z-axis is assumed to be continuous across the surface. Then, our principle (equation (2)) takes the form

$$\begin{aligned}\mathtt{min}\ \mathtt{F} &= \tfrac{1}{2}\sum_{j,m}\left(\phi_j M^{\Phi}_{j,m}\phi_m + \zeta_j M^{\mathrm{Z}}_{j,m}\zeta_m\right)\\ &- \sum_{j,m}\left(\check{\phi}_j M^{\Phi}_{j,m}\phi_m + \check{\zeta}_j M^{\mathrm{Z}}_{j,m}\zeta_m\right)\\ &+ N\alpha\sum_j j^2\phi_j.\end{aligned} \tag{5}$$

Above, we have used

$$\alpha \equiv f h_{\mathrm{c1,g}}\left[\frac{\check{\imath}+\mathrm{inc}}{\sqrt{1+(\check{\imath}+\mathrm{inc})^2/4h_0^2}} - \frac{\check{\imath}}{\sqrt{1+\check{\imath}^2/4h_0^2}}\right].$$

Lower case emphasizes the use of dimensionless units. Thus, we have introduced $h_0 \equiv H_0/(J_{\mathrm{c}}R)$, $h_{\mathrm{c1,g}} \equiv H_{\mathrm{c1,g}}/(J_{\mathrm{c}}R)$, and $\imath \equiv I/(J_{\mathrm{c}}\pi R^2)$. 'inc' denotes the transport current increment.

5. Discussion

Figure 5 displays the results of applying our theory to the case $h_0 = 2$ and $f h_{\mathrm{c1,g}} = 1$, for FC and ZFC conditions. As one can notice both in the experimental results and theoretical calculations, the longitudinal magnetic moment of the superconducting cylinder *collapses* towards the equilibrium magnetization curve. Thus, successive cycles of the applied transport current increase the longitudinal diamagnetic moment, corresponding to the decrease of trapped magnetic field during the FC process. In contrast, the ZFC curve displays a decrease of the diamagnetic moment, related to the reduction of Bean shielding currents in this case. The previous facts may be explained in terms of our isotropic critical state model, as a competition between the longitudinal and azimuthal components of the current density (J_z, J_ϕ). The

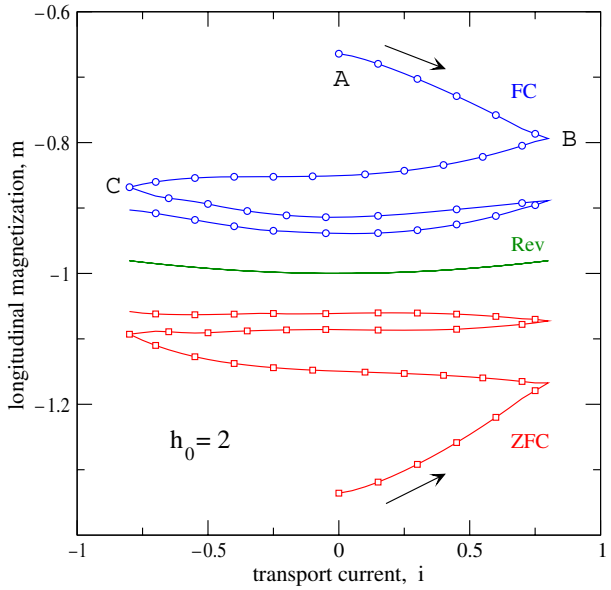

Figure 5. Theoretical estimates for the field cooled and zero-field-cooled magnetization under transport current cycles in a superconducting cylinder with the influence of equilibrium magnetization effects. Dimensionless units have been used, defined in terms of the irreversible magnetization for zero applied current (see text).

actual distribution rule depends on the restriction $J_z^2+J_\phi^2 \leqslant J_c^2$ and Faraday's law, which enhances the component that shields the induced field changes.

Let us analyse the situation in which the sample has been cooled in a magnetic field. The numerical simulations provide a prediction for the circulating volume current density within the sample. Figures 6 and 7 illustrate the flux dynamics in the first branches of the current cycles. Initially, the sample holds a noticeable amount of trapped longitudinal flux, with a corresponding density profile $J_\phi = J_c$ and $J_z = 0$. Then, as the transport current is increased ($J_z \neq 0$ in figure 6), the shielding capability decreases, and this leads to flux expulsion (J_ϕ is reduced from the surface).

When the transport current changes are reversed ($B \rightarrow C$ in figure 7), we recall that Faraday's law enhances a maximum negative transport close to the sample's surface. The high value of J_z implies a noticeable reduction of J_ϕ, and thus a further reduction of trapped flux. In passing, one can realize that the transition of J_z from positive to negative values produces a peak structure in J_ϕ, as related to the condition $J_z^2 + J_\phi^2 = J_c^2$, i.e. $J_z = 0 \Rightarrow J_\phi = J_c$. The failure of our simulation in obtaining this exact rule is ascribed to numerical error when the peak structure is very sharp.

The general trend of developing a transport critical state ($J_z \rightarrow \pm J_c$) as the transport current is further cycled may be observed. As a consequence, the *Bean* shielding current is irreversibly reduced to negligible values, and the sample's magnetic moment is determined by the equilibrium magnetization, which has been modelled as a jump in the magnetic field at the boundary.

6. Conclusions

Irreversible magnetization collapse towards the equilibrium state is reported in the longitudinal current problem for field cooled and zero-field-cooled experiments. Measurements have been performed in YBCO cylindrical samples, close to the critical temperature ($0.75 < T/T_c < 0.95$) and around and above the dissipation threshold, when both the applied magnetic field and the transport current were directed along the axis of the sample.

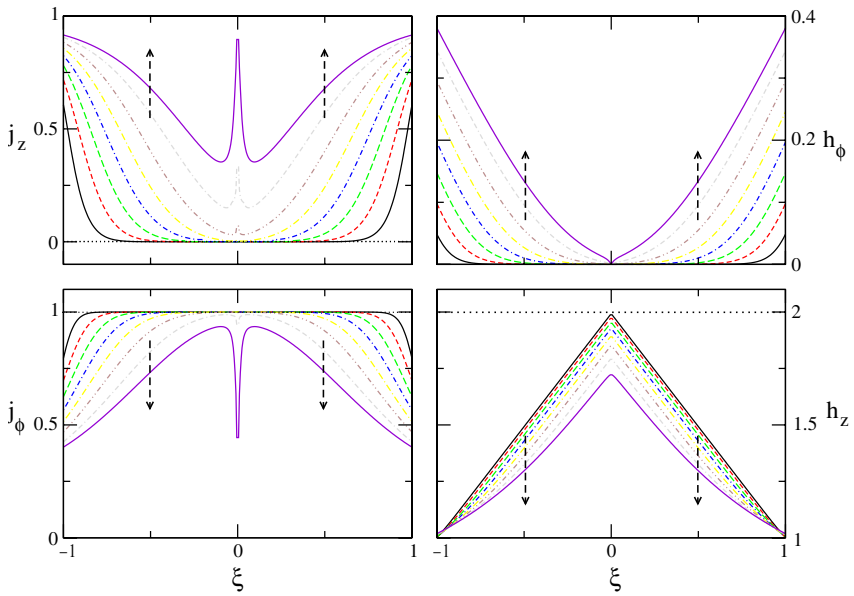

Figure 6. (Left) Theoretical estimate of the current density distribution within the superconductor for the first branch of the transport cycle (A → B in figure 5). The dashed arrows indicate the evolution of the profiles as the applied current is changed. To the right, the corresponding field profiles are shown. Simulations correspond to an applied field strength $h_0 = 2$ (see text for units). The horizontal axis displays the artificial variable $-r/R < \xi < r/R$, so as to plot a longitudinal section of the sample.

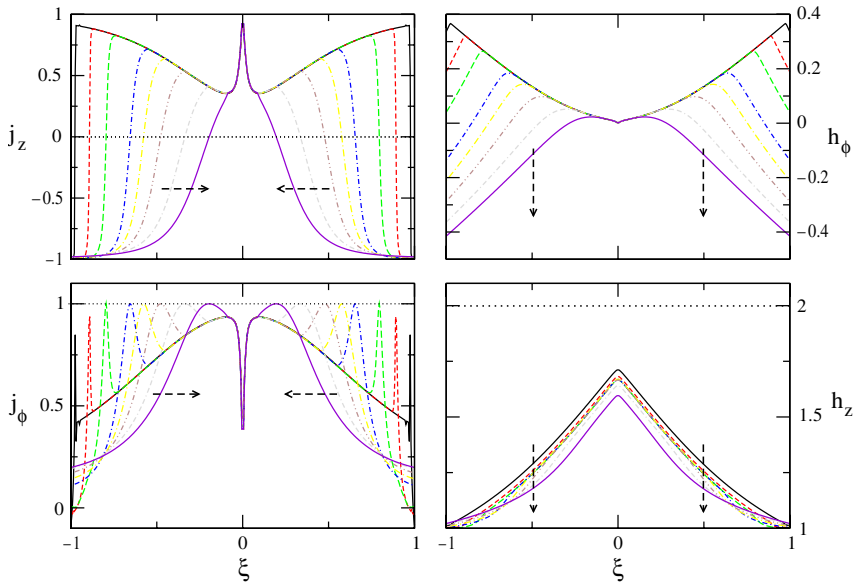

Figure 7. The same as figure 6 for the second branch of the transport cycle (B → C in figure 5), where the transport current has been reversed.

The generalized critical state theory, modified so as to include reversible magnetization effects, allows us to explain the main features of the experimental observations. The longitudinal flux profiles within the sample develop a decreasing slope as transport current is applied, because of the current density limitation ($\|\vec{J}\| \leqslant J_c$). In the FC case this leads to the expulsion of trapped flux. In the ZFC case, flux penetration is induced. Both phenomena lead to the *consumption* of irreversible magnetization.

Acknowledgments

This work was partially supported by Chilean FONDECyT projects 1040668, 7040043 and 7050089, Argentina ANPCyT PICT00-03-08937, Spanish CICyT project BFM2003-02532, and the Research Groups Budget of the local government (Aragón, Spain).

Appendix A. Mutual inductance matrix

Here, we show that the variational statement in equation (1) may be transformed into a quadratic function optimization problem, by means of the mutual inductance matrix concept. We first focus our attention on the term

$$\int_\Omega H^2 \, \mathrm{d}V = \int_\Omega \left(H_\varphi^2 + H_z^2\right) \, \mathrm{d}V.$$

Let us separate the azimuthal and z components, and transform the previous equation in terms of the related current densities. For this purpose, we discretize the cylinder in a set of layers, each of length L, thickness δ and average radius r_j. Following the notation introduced in the text, we assume that a current density $(0, \phi_j, \zeta_j)$ flows along a given layer. Next, we write the field components in terms of the current density, making use of Ampère's law. We treat each case separately.

A.1. Azimuthal magnetic field contribution

Notice that, at a given distance r_j, we have

$$H_\varphi(r_j) \approx \delta \left(\frac{1}{2}\zeta_j + \sum_{m<j} \frac{r_m}{r_j}\zeta_m\right). \tag{A.1}$$

Then, the integration may be discretized as

$$\int_\Omega H_\varphi^2 \, \mathrm{d}V \approx 2\pi L\delta^3 \sum_{j=1}^{N} r_j \left(\frac{1}{2}\zeta_j + \sum_{m<j} \frac{r_m}{r_j}\zeta_m\right)^2. \tag{A.2}$$

Now, by using the integer number representation $r_j = j\delta$ and by inspection of the first terms in the arising series, one can rearrange the summation in the form

$$\begin{aligned}\int_\Omega H_\varphi^2 \, \mathrm{d}V &\approx 2\pi L\delta^4 \sum_j \left(\frac{j}{4} + j^2 \sum_{k=j+1} \frac{1}{k}\right)\zeta_j\zeta_j \\ &\quad + 2\pi L\delta^4 \sum_{j\neq m} \left(\frac{1}{2}\mathtt{min}\{j,m\} + jm \sum_{k=\mathtt{max}\{j,m\}+1}^{N} \frac{1}{k}\right)\zeta_j\zeta_m \\ &\equiv \sum_{j,m} \zeta_j M^{\mathrm{Z}}_{j,m} \zeta_m,\end{aligned} \tag{A.3}$$

which is nothing but the desired mutual inductance expression. Recall that $M^{\mathrm{Z}}_{j,m}$ is an array of geometrical coefficients, which one can calculate at once, and further use for a definite physical process in the cylinder.

A.2. Axial magnetic field contribution

The procedure is quite similar to the previous case. Now, we start by noticing that the axial magnetic field at a given distance r_j may be approximated by

$$H_z(r_j) \approx H_0 + \delta \left(\frac{\phi_j}{2} + \sum_{m>j} \phi_m\right) \tag{A.4}$$

with H_0 the given applied magnetic field. Thus

$$\int_\Omega H_z^2 \, \mathrm{d}V \approx 2\pi L\delta^3 \sum_{j=1}^{N} r_j \left(H_0 + \delta \frac{\phi_j}{2} + \sum_{m>j} \phi_m \right)^2 . \quad \text{(A.5)}$$

Again, by expanding the summations, one can notice that

$$\begin{aligned}
\int_\Omega H_z^2 \, \mathrm{d}V \approx{}& 2\pi L\delta^4 \sum_j \left(\frac{j(j-1/2)}{2} \right) \phi_j \phi_j \\
&+ 2\pi L\delta^4 \sum_{j\neq m} \left(\tfrac{1}{2} \left[\min\{j,m\} \right]^2 \right) \phi_j \phi_m \\
&+ 2\pi L\delta^4 \sum_j \left(\frac{H_0}{\delta} j^2 \right) \phi_j \\
&+ 2\pi L\delta^4 \left(\frac{H_0}{\delta} \right)^2 \frac{N(N+1)}{2} \\
\equiv{}& \sum_{j,m} \phi_j M^{\Phi}_{j,m} \phi_m + \sum_j N^{\Phi}_j \phi_j + F_0 . \quad \text{(A.6)}
\end{aligned}$$

Above, the *constant* term F_0 has been emphasized, as it is not dependent on the actual current distribution within the sample, and may be dropped for minimization purposes.

References

[1] Bean C P 1964 *Rev. Mod. Phys.* **36** 31
[2] Clem J R 1982 *Phys. Rev.* B **26** 2463
[3] J R Clem and Hao Z 1993 *Phys. Rev.* B **48** 13774
[4] Brandt E H 1992 *Physica* C **195** 1
[5] Tinkham M and Lobb C J 1989 *Solid State Physics* (Singapore: World Scientific)
[6] Dersch H and Blatter G 1988 *Phys. Rev.* B **38** 11391
[7] LeBlanc M A R and Celebi S 2003 *Supercond. Sci. Technol.* **16** 329
[8] Boyer R, Fillion G and LeBlanc M A R 1980 *J. Appl. Phys.* **51** 1692
[9] Clem J R and Pérez-González A 1984 *Phys. Rev.* B **30** 5041
[10] Clem J R and Pérez-González A 1986 *Phys. Rev.* B **33** 1601
[11] Badía A, López C and Giordano J L 1998 *Phys. Rev.* B **58** 9440
[12] Badía A and López C 2001 *Phys. Rev. Lett.* **87** 127004
[13] Giordano J L and Angurel L A 2001 *Supercond. Sci. Technol.* **14** 655
[14] Pérez-Rodríguez F, Pérez-González A, Clem J R, Gandolfini G and LeBlanc M A R 1997 *Phys. Rev.* B **56** 3473
[15] Ginzburg S L, Gerashchenko O V and Sibilev A I 1997 *Supercond. Sci. Technol.* **10** 395